1962

A Theory of Space Probe Entry Near the Low-Meteoric Velocity Limit

Frederick Cyril Grant
College of William & Mary - Arts & Sciences

A THEORY OF SPACE PROBE ENTRY NEAR THE LOW-METEORIC VELOCITY LIMIT

A Thesis

Presented to

The Faculty of the Department of Physics

The College of William and Mary in Virginia

In Partial Fulfillment

Of the Requirements for the Degree of

Master of Arts

By

Frederick Cyril Grant

August 1962

APPROVAL SHEET

This thesis is submitted in partial fulfillment of

the requirements for the degree of

Master of Arts

Frederick Cyril Cronk

Author

Approved, August 1962:

Robert E. Smith

Robert E. Smith, M.A.

John L. McKnight

John L. McKnight, Ph.D.

Donald E. McLennan

Donald E. McLennan, Ph.D.

F. P. Cromfield, Jr.

TABLE OF CONTENTS

LIST OF FIGURES

ABSTRACT

A theory of velocity limitation is developed on the basis of a simple analytical model of a returning space probe. The limiting velocity is that atmospheric entry speed for which the probe is entirely consumed. The geometry treated is a family of slender blunted cones moving in the direction of the axis. The face of the cone is assumed to be continuously vaporized by the flow. The entry speed is presumed so high that a large fraction (or all) of the vehicle volume is consumed in the entry. The entry speed is also large enough that the dominant mode of heat transfer to the vehicle is through radiation from the hot gas cap at the nose. In the regime of radiation dominance, a second-order nonlinear differential equation is found which describes the geometrical and dynamical history during atmospheric entry. By means of solutions of the basic size-altitude equation the low-meteoric velocity limit is traced out.

For the family of truncated cones, and a limiting form of the heat input function, explicit formulas for the limiting velocity are developed. The limiting velocity is found to be independent of the size of the probe, but dependent on the shape. Pointed cones yield the highest limiting velocities for the class of probes considered. However, flat-faced cylinders yield values nearly as high. The proportions of the cylinders do not affect the limiting velocity so that long rods and thin wafers have the same values. Only the altitude of the high mass-loss region shifts with the probe size or with the cylinder proportions.

A THEORY OF SPACE PROBE ENTRY NEAR THE LOW-METEORIC VELOCITY LIMIT

INTRODUCTION

Even now, in the space age, the only bodies entering the atmosphere with sufficient velocity to suffer large fractional mass loss are the natural meteors. Ballistic missiles and the current space vehicles typically do not devote but a few percent of their mass to combating heat flux. Even return from the moon will not require too much larger heat protection weights than do earth satellites. Only in the entry speed range of returning space probes do mass losses approach complete consumption of the vehicles.

The speeds corresponding to the different regimes of atmospheric entry are as follows: ballistic missiles at about 20,000 feet per second; near-earth satellites at about 26,000 feet per second; lunar return vehicles at about 36,000 feet per second; meteors and space probes above 36,000 feet per second. Only in the case of meteors and space probes is there a broad band of speeds ranging, for meteors, up to 45 miles per second for head-on collision with a meteor on a parabolic orbit with respect to the sun.

For minimum energy orbital transfer from the distance of the earth to the distance of Pluto a launch velocity of about 53,000 feet per second is required, only slightly less than that for escape from the sun's gravitational field. The corresponding transit time is about 46 years. Except for minimum energy return the entry speeds will exceed the launch speeds. To shorten round-trip times it is important to know the limiting speeds at which man-made vehicles may enter the atmosphere and survive.

The basic contrasts between the cases of meteor and probe entry lie in the sizes, materials, and shapes. Meteorites come in two materials, iron and stone; reach enormous sizes, and seem to have irregular, blunt shapes. Probes, on the other hand, cannot weigh more than a few thousands of pounds, and the materials and shapes can be chosen as desired. For successful probes a definite fraction of the mass, the scientific payload, must survive the entry. Of course, in a sense, a meteorite is intrinsically a scientific payload.

The anticipated speeds of probe entry are well beyond the capability of shock tubes. Shock tubes are unlikely to achieve speeds much higher than the present limit of about 40,000 feet per second. Information on entry at higher speeds can, at present, be directly obtained only by observation of meteors. Recourse must be made to judicious extrapolation and to analytical methods for investigation of space probe entry.

The problem of natural meteor mechanics has been successfully treated, in the main, without detailed consideration of the heat input function. (Ref. 1, for example.) Although shock tube experiments and theoretical analyses have produced realistic heat input functions for simple shapes and it is now possible to include realistic heat input functions in problems of entry mechanics, the range of applicability of the results for high mass-loss trajectories is not known.

A critical regime in space probe return is found near the low-meteoric velocity limit, the existence of which was suggested in reference 2. On the analysis of reference 2, meteor-like bodies in the ballistic parameter range of interest for space probes ($\sim 10^2$ psf) are completely consumed for entry velocities higher than roughly 50 to 60 thousand feet per second.

It is the purpose of this paper to develop the theory of velocity limitation for probe-like bodies. This means a choice of physically reasonable shapes must be made and the survival of a definite fraction of the initial mass must be provided.

CHAPTER I

ANALYSIS OF MOTION AND HEATING

1.1 Dynamical Equation

The velocities and air loads are so high for the cases to be considered that the acceleration of gravity will be neglected. Only after the nearly coincident heat, mass-loss, and acceleration pulses are over will gravity have any importance to the motion. Neglect of gravity implies that the motion is linear. Another simplifying assumption is that the entry is at such a steep angle that the curved surfaces of constant atmospheric density may be regarded as parallel planes for the straight flight paths to be considered. The atmosphere is to be approximated by an isothermal model at constant acceleration of gravity. Such a model has an exponential variation of density with altitude which may be expressed as

$$\frac{d\rho}{\rho} = -\frac{dh}{h_s} \qquad 1.1.1$$

The parameter, h_s, which fixes the decrement of density with altitude on the isothermal model is called the scale height of the atmosphere. In the nonisothermal atmospheric model of reference 3, local values of scale height are tabulated. The parameter h_s may be defined as the altitude change for which the density changes by the factor e, the base of natural

logarithms. For the simplified atmpspheric entry model under discussion, a generalized scale height, h_s', may be defined as the distance along the flight path in which the density changes by the factor e. The two parameters are related simply by

$$\sin \gamma \cdot h_s' = h_s \qquad 1.1.2$$

where γ is the angle of the flight path with the horizontal.

The substitution of the density for time as independent variable will be made as a matter of convenience. In terms of the relations 1.1.1 and 1.1.2 we find

$$d\rho = \frac{\rho U}{h_s'} dt \qquad 1.1.3$$

as the relation between t and ρ. The equation of motion becomes on the assumptions outlined above

$$-\frac{dU}{d\rho} = \frac{gh_s'}{2\delta} U \qquad 1.1.4$$

where $\delta = mg/C_D A$ is the so-called ballistic parameter. Depending on the geometry chosen, the coefficient of U on the right member of equation 1.1.4 is an, as yet, unspecified function of the nondimensional size, λ, of the probe. This functional relationship will be denoted as

$$f(\lambda) = \frac{gh_s'}{2\delta} \qquad 1.1.5$$

so that the equation of motion has the form

$$-\frac{dU}{d\rho} = f(\lambda) \cdot U \qquad 1.1.6$$

Axial symmetry of the probe is assumed and the aerodynamic drag will be computed on the so-called Newtonian hypersonic approximation. Each of the flux of particles impinging on the vehicle is considered to strike the vehicle independently, losing the velocity component normal to the body as it does so. For the continuum flow under consideration, the shock wave at hypersonic speeds is so closely wrapped about the nose of the body that the Newtonian assumptions are closely realized.

1.2 Heating Equation

The relationship of λ to ρ is found by relating the surface heat input to the change in volume produced by it. The precise form of this relation will be given later in terms of specific models. For the present it will merely be noted that the relation will be a special case of the form

$$-\frac{d\lambda}{d\rho} = \rho^{r-1} \cdot U^{s-1} \cdot g(\lambda) \qquad 1.2.1$$

1.3 Size-Altitude Equation

The analysis takes a compact form if the equations 1.1.6 and 1.2.1 are combined. By differentiation of equation 1.2.1 and substitution of equation 1.1.6, the following second-order size-altitude equation is found which is the basic equation of the present analysis

$$\frac{d^2\lambda}{d\rho^2} + \left\{(s-1)f(\lambda) - \frac{r-1}{\rho}\right\}\frac{d\lambda}{d\rho} - \frac{g'(\lambda)}{g(\lambda)}\left(\frac{d\lambda}{d\rho}\right)^2 = 0 \qquad 1.3.1$$

An advantage of equation 1.3.1 is that it is independent of the velocity which appears explicitly only in the boundary condition

$$-p = -\frac{d\lambda}{d\rho} = \rho^{r-1}U^{s-1}g(\lambda) \qquad 1.3.2$$

It is, for many purposes, more convenient to write equations 1.3.1 in terms of the variable $\omega = \ln\rho$ which is linearly related to the altitude in an isothermal atmosphere at constant g. The transformation yields

$$\frac{d^2\lambda}{d\omega^2} + \left\{(s-1)e^{\omega}f(\lambda) - r\right\}\frac{d\lambda}{d\omega} - \frac{g'(\lambda)}{g(\lambda)}\left(\frac{d\lambda}{d\omega}\right)^2 = 0 \qquad 1.3.3$$

$$-\pi = -\frac{d\lambda}{d\omega} = e^{r\omega}U^{s-1}g(\lambda) \qquad 1.3.4$$

In the form of equations 1.3.3 and 1.3.4 the size-altitude equation indicates some general properties of the solutions which lead to scaling laws for various physical quantities with various physical parameters. For example, for parameters which appear as factors of $g(\lambda)$, but do not appear in $f(\lambda)$, variation of these factors with no change in the product produces no change in the integral curve.

A more general transformation is the change of the integral curves under the variation of any parameter z which appears as a factor of $f(\lambda)$. If we imagine an element of arc of an integral curve of equation 1.3.3 to be translated in ω by an amount σ so that

$$\omega' = \omega + \sigma$$

The coefficient of the linear term in $\frac{d\lambda}{d\omega}$ of equation 1.3.3 undergoes the change

$$ze^{\omega} \rightarrow z'e^{\omega'} = z'e^{\sigma}e^{\omega}$$

where $z \rightarrow z'$ in the translation. If we require of z' that

$$z = z'e^{\sigma} \qquad 1.3.5$$

then the $\frac{d^2\lambda}{d\omega^2}$ term of differential equation 1.3.3 is unchanged for the translated element. Thus any integral curve, when translated, is a solution for a different value of z. The functional dependence of certain quantities of interest follows directly from this invariance of the integral curves under a translation σ plus an associated change of z. Written in a form different from equation 1.3.5 the proper association is

$$\rho z = \text{constant} \qquad 1.3.6$$

The transformation described by equations 1.3.5 or 1.3.6 will be called a σ-z change.

The character of the integral curves of the size-altitude equation 1.3.3 for physically interesting cases is indicated in figure 1. Two semi-infinite regions of nearly constant size are separated by a region of rapid size change, the high mass-loss region. In this narrow region occurs the heating pulse, the acceleration pulse, and the size change $\left(-\frac{d\lambda}{d\omega}\right)$ pulse which peaks at point i, the inflection point. The acceleration pulse peaks at point G which follows the inflection point. The limiting

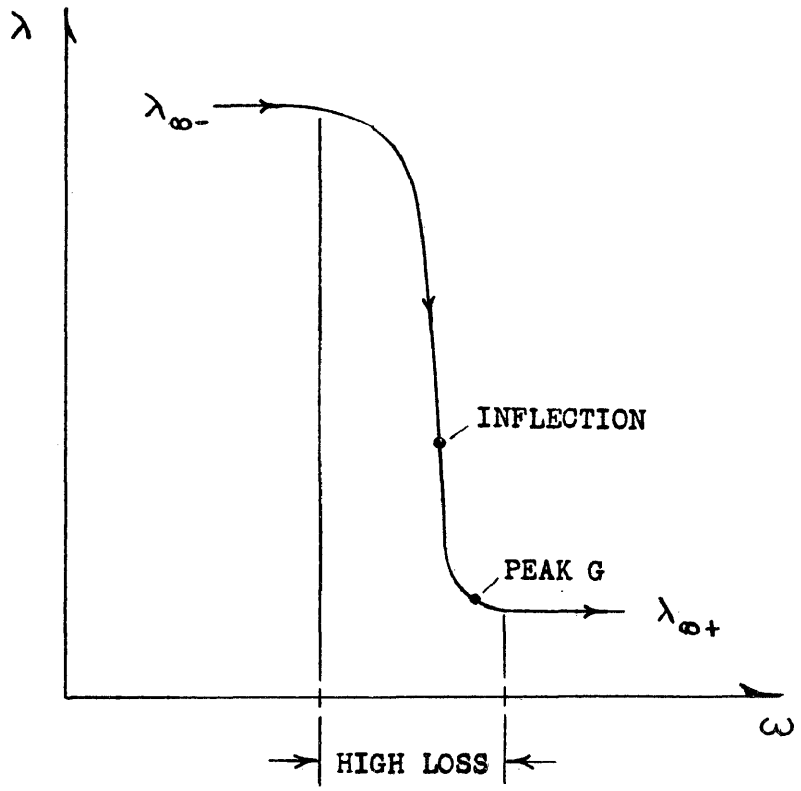

Figure 1.- Sketch of integral curve of size-altitude equation.

velocity is defined in terms of the limiting size on the right, $\lambda_{\omega+}$. The velocity, $U_{\omega-}$, at $\omega = -\infty$ for which $\lambda_{\omega+} = 0$ is defined as the limiting velocity, U_l. For higher velocity at $\omega = -\infty$ the vehicle will burn up at finite altitudes (unless the payload vanishes, which case, corresponding to meteor-like bodies, will be discussed later).

Although the size-altitude equation can be regarded as a geometrical relation, the terms have dynamical significance. The only term unequivocally favorable to probe survival is that with f as coefficient, corresponding to loss of velocity and mass during entry. High values of f are desirable, or alternatively, small values of $\delta_{\omega-}$ are desirable. More precisely, as will be seen later, it is a high mean value of δ^{-1} that is desirable.

1.4 Heat-Input Function

For coordinates moving with the body, the flux of kinetic energy of the impinging air is

$$\tfrac{1}{2} \rho U^3 \qquad 1.4.1$$

per unit area. This energy may be regarded as an upper bound for the heat input to the body, or as the unit of heat input. In terms of this unit, the heat input per unit frontal area may be written

$$\dot{Q} = \eta \tfrac{1}{2} \rho U^3, \quad \eta \leq 1 \qquad 1.4.2$$

Detailed theoretical considerations and experiments have yielded heat input functions for the stagnation point regions of blunt bodies. These relations hold for the two distinct components of heat input: the convective, and the radiative. The convective component is due to the

frictional action of the air. It can be shown to have the functional form (for example, ref. 4)

$$q_{sc} \propto \sqrt{\rho}\, U^3 \frac{1}{\sqrt{x}} \qquad 1.4.3$$

for the energy input per unit area at the stagnation point where x is a characteristic length of the body. The decrease in rate with size does not mean that the heat input will vanish at infinite size, since the integrated input varies as $x^{3/2}$.

The radiative component is caused by the shock wave which raises the enthalpy of a unit mass of air by about $\frac{1}{2}\rho U^2$ near the stagnation point. At space probe velocities, this amount of energy is sufficient to put the equilibrium temperature at such high values ($\sim 10^4$ °K) that ionization and dissociation are important. The inverse recombination processes produce the important radiation, particularly the Kramers recombination of atomic nitrogen ions and electrons (ref. 5). For the radiative component it is found experimentally that (ref. 6)

$$q_{sr} \propto \rho^2 U^{14} x \qquad 1.4.4$$

The enormous increase with velocity and the sharp rise with density should be noted in relation 1.4.4. The rates of increase are more rapid than in the limiting energy flux indicated by equation 1.4.2 so that clearly the relation 1.4.4 cannot hold to arbitrarily large densities and velocities. Also, the heating rate cannot increase indefinitely with size, x. Although the hot gas cap volume increases nearly in direct proportion to size,

there cannot be a substantial increase in heating rate beyond the size for which the shock stand-off distance is comparable to the gas cap self-absorption length.

However, the indicated large increases of radiative heating with density and velocity suggest that radiation becomes the dominant form of heat transfer with increasing entry speeds. This is, indeed, the case; and the analysis of the present paper will consider the regime in which the integrated contribution of the convective heat transfer may be neglected in comparison with the integrated radiative transfer. The experimental variation 1.4.4 will be followed until it is necessary to impose the limiting form as is suggested by considerations of energy conservation.

A perhaps important, but certainly complicated, phenomenon which is neglected throughout the analysis is the effect on the motion of the vaporized probe material. Under the presumed high mass-loss conditions the vaporized layer of probe material may be a significant fraction of the shock layer with important effects. One effect is likely to be a reduction of uncertain magnitude in the convective heating. However, convection in its undiminished form is negligible in the regime of interest so that any decrease in convection is unimportant. With respect to radiation, the shielding or intensifying effects of the boundary layer of probe material must be put down as a neglected, but perhaps significant, quantity.

CHAPTER II

ANALYTICAL MODEL

2.1 General Description

In view of the fact that high radiation intensities are associated with the large enthalpy changes in normal shock waves, and that radiative heat transfer is increasingly dominant at space probe (meteoric) speeds, it seems desirable that the surfaces of space probes should have small fractions of the surface area exposed to strong shock waves. This suggests that the basic shape of space probes, unlike that of meteors, should be slender so that strong shock waves can exist only at the foremost parts. A slender blunted cone suggests itself as a possibility since the area of the blunted nose will increase with mass loss and the drag will thus increase at the lower velocities for which radiation intensity is lessened. Detailed analysis will show if these simple considerations are justified.

For the conical model to be considered (fig. 2) the nose is considered to be initially planar, and to remain so, although it is recognized that there will be rounding at the edges. Since the intensity of heat transfer will be greatest at the stagnation point, an initially blunt nose will remain blunt, and minor changes at the shoulders will not significantly affect the dynamical and heating history.

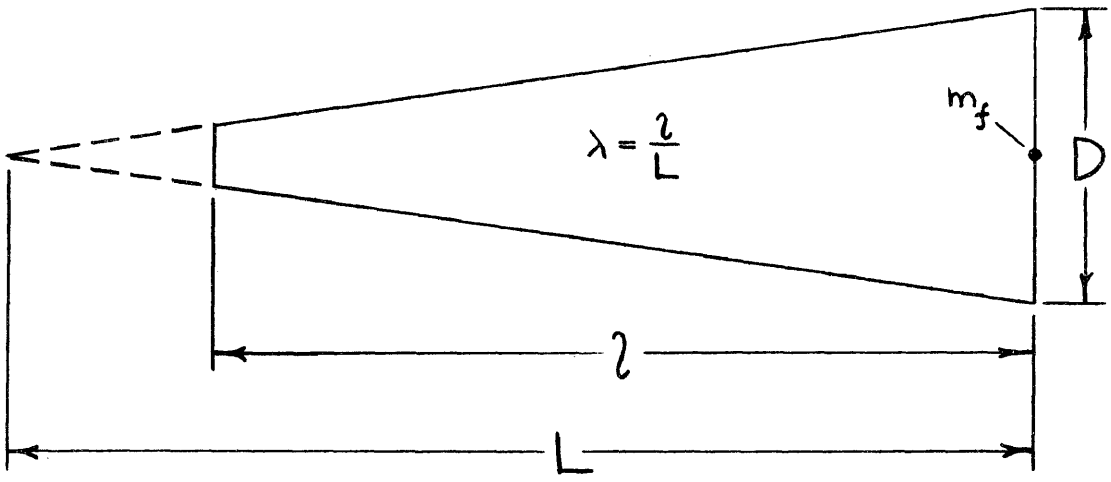

Figure 2.- Sketch of blunted cone.

2.2 Ballistic Function, f

The, until now, unspecified function f is found for the assumed flat-faced slender cone by evaluation of the weight and C_DA in terms of the assumed geometry. By a simple integration the quantity C_DA is found to be

$$C_DA = \frac{\pi}{2} D^2 \left\{ \frac{(1-\lambda)^2 + \left(\frac{D}{2L}\right)^2}{1 + \left(\frac{D}{2L}\right)^2} \right\} \qquad 2.2.1$$

The weight of the probe is easily found to be

$$mg = wV + m_p g = \frac{\pi}{3} wL^3 \left(\frac{D}{2L}\right)^2 \left[1 - (1-\lambda)^3\right] + m_p g \qquad 2.2.2$$

with V, the probe volume; w, the weight density; and m_p, the payload. The function f thus becomes

$$f(\lambda) = \frac{gh'_s}{2\delta} = 3 \frac{gh'_s}{wL} \cdot \frac{1}{\frac{1}{1-\mu} - (1-\lambda)^3 - \frac{\mu}{1-\mu}(1-\lambda_\infty)^3} \cdot \frac{(1-\lambda)^2 + \left(\frac{D}{2L}\right)^2}{1 + \left(\frac{D}{2L}\right)^2} \qquad 2.2.3$$

where $\mu = \frac{m_p}{m_\infty}$ is the payload fraction, and λ_∞ is the initial nondimensional size.

2.3 Heating Function, g

The other unspecified function g is fixed by equation of the heat input to the heat capacity of the evaporated material. At first the equation will be written with both convective and radiative terms. One finds

$$-\frac{dV}{d\lambda}\hat{\lambda} = \frac{1}{w\,\Delta W}\int (q_r + q_c)dS = \frac{1}{w\,\Delta W}\left\{\left(\frac{\tilde{q}}{q_s}\right)_c q_{sc} + \left(\frac{\tilde{q}}{q_s}\right)_r q_{sr}\right\} S_{face} \qquad 2.3.1$$

Introducing the experimental forms of the heat input functions one finds

$$-\frac{d\lambda}{d\rho} = \frac{h_s'}{w\,\Delta W}\left\{\left(\frac{\tilde{q}}{q_s}\right)_c \frac{\alpha}{L^{3/2}\sqrt{\frac{D}{L}}}\rho^{m-1}U^{n-1}\frac{1}{\sqrt{1-\lambda}} + \left(\frac{\tilde{q}}{q_s}\right)_r \beta\left(\frac{D}{L}\right)\rho^{r-1}U^{s-1}(1-\lambda)\right\} \qquad 2.3.2$$

where the characteristic length x, is the face diameter. The constants α and β in equation 2.3.2 correspond to unit face diameter. As previously mentioned, for sufficiently high velocity the radiative contribution will be dominant and for sufficiently low speeds the convection will dominate. The case to be considered is that in which the contribution of the radiative term is dominant. Suppression of the convective term of equation 2.3.2 yields the result

$$-\frac{d\lambda}{d\rho} = K\rho^{r-1}U^{s-1}(1-\lambda) \qquad 2.3.3$$

where

$$K = \frac{h_s'}{w\,\Delta W}\left(\frac{\tilde{q}}{q_s}\right)_r \beta\left(\frac{D}{L}\right) \qquad 2.3.4$$

so that

$$g(\lambda) = K(1-\lambda) \qquad 2.3.5$$

The size-altitude equation 1.3.3 becomes

$$\frac{d^2\lambda}{d\omega^2} + \left\{(s-1)e^{\omega}f(\lambda) - r\right\}\frac{d\lambda}{d\omega} + \frac{1}{1-\lambda}\left(\frac{d\lambda}{d\omega}\right)^2 = 0 \qquad 2.3.6$$

For $r = 2$ and $s = 14$, with a β value estimated from the results of reference 6, numerical integrations of equation 2.3.6 have shown that for steep entry and high mass-loss, the radiative heat inputs indicated by the radiative term of equation 2.3.2 exceed the kinetic energy available in the flow except at the beginning and at the end of the trajectory. For completeness, however, the trajectory properties corresponding to equation 2.3.6 are indicated in the appendix.

A physically acceptable radiative heat flux cannot exceed the flux of kinetic energy onto the face of the probe. This flux is

$$\frac{1}{2}\rho U^3 \qquad 1.4.1$$

per unit area. Recalling that the limiting radiative heat flux can be written as

$$\dot{q} = \eta\,\frac{\rho}{2}\,U^3 \qquad 1.4.2$$

an upper bound to the radiant heat flux is found if one assumes, in coordinates moving with the probe, that all the incident energy flux is converted to photons, half of which enter the body and half escape. The assumptions require that

$$\eta \leq \frac{1}{2} \qquad 2.3.7$$

so the radiative heat input cannot exceed half the kinetic energy flux. Because of the small range of validity of equation 2.3.6 on the high mass-loss trajectories to be considered, the heat input function 1.4.2 will be adopted. The size-altitude equation corresponding to the function 1.4.2 has the simple form

$$\frac{d^2\lambda}{d\rho^2} + 2f \frac{d\lambda}{d\rho} = 0 \qquad 2.3.8$$

or

$$\frac{d^2\lambda}{d\omega^2} + \left\{2\rho f - 1\right\} \frac{d\lambda}{d\omega} = 0 \qquad 2.3.9$$

with

$$- \frac{d\lambda}{d\rho} = K'U^2 \qquad 2.3.10$$

or

$$- \frac{d\lambda}{d\omega} = K'\rho U^2 \qquad 2.3.11$$

for

$$K' = \frac{h_s'}{v\,\Delta W} \cdot \frac{1}{2L} \qquad 2.3.12$$

2.4 Limiting Velocity

For the separable equation 2.3.8, a first integral may be obtained by quadrature as

$$p + 2\int f d\lambda = \text{constant} \qquad 2.4.1$$

and a second integral as

$$\rho + (\text{constant})' = \int \frac{d\lambda}{(\text{constant}) - 2\int f d\lambda} \qquad 2.4.2$$

If we define

$$F(\lambda) = 2\int_0^{\lambda} f d\lambda \qquad 2.4.3$$

we find the first integration constant in terms of entry conditions as

$$\text{constant} = F(\lambda_{\infty_-}) - K' U_{\infty_-}^2 \qquad 2.4.4$$

The limiting velocity is found directly as the value of U_{∞_-} corresponding to $p = 0$ at $\lambda = 0$.

$$U_l^2 = \frac{F(\lambda_{\infty_-})}{K'} \qquad 2.4.5$$

On a σ-z change it is found that the limiting velocity is independent of size, L; weight density, w; and effective scale height, h_s'. In fact, the only indicated dependence is the following

$$\frac{\partial \log U_1}{\partial \log\left(\frac{\Delta W}{\eta}\right)} = \frac{1}{2} \qquad 2.4.6$$

2.5 Dynamical Quantities

It is convenient to express the deceleration, G, and velocity, U, in terms of the solutions $\lambda(\rho)$. For the velocity we find

$$U^2 = \frac{-\frac{d\lambda}{d\rho}}{K'} \qquad 2.5.1$$

and for the dimensionless acceleration

$$G = -\frac{\dot{U}}{g} = \frac{\rho f}{g h_s'} U^2 \qquad 2.5.2$$

The peak acceleration occurs on the condition

$$\dot{G} = \frac{dG}{d\rho}\dot{\rho} = 0 \qquad 2.5.3$$

Differentiating the right member of equation 2.5.2 with respect to ρ and setting derivative to zero one finds at the peak G condition

$$2\rho f = 1 + \frac{d \ln f}{d\lambda} \cdot \frac{d\lambda}{d\rho} \geq 1 \qquad 2.5.4$$

Relation 2.5.4 is a generalization of that of the analysis of reference 7 which treats the case of constant size and shape, finding $2\rho f = 1$ at peak G.

2.6 Limiting Velocity Formulas

For the class of slender blunted cones the limiting velocity can be evaluated in closed form in terms of elementary functions. Only the case

of limiting velocity will be considered so that the integration constant of equation 2.4.1 is zero when F is used for the integral on the left-hand side. For the function F one finds

$$F(\lambda) = \frac{2gh'_s}{wLb^{2/3}}(1 + a)^{-1}\left[-b^{2/3}\ln(b - x^3) - a\ln\frac{b^{1/3} - x}{\sqrt{b^{2/3} + b^{1/3}x + x^2}}\right.$$

$$\left. + \sqrt{3}\, a \tan^{-1}\frac{\sqrt{3}\, x}{2b^{1/3} + x}\right]_{1-\lambda}^{1} \qquad 2.6.1$$

where

$$a = \left(\frac{D}{2L}\right)^2 \geq 0$$

$$b = \frac{1}{1 - \mu}\left[1 - \mu(1 - \lambda_{\infty-})^3\right] \geq 1$$

and for limiting velocity

$$U_l^2 = 4g\frac{\Delta W}{\eta}\frac{(1 + a)^{-1}}{b^{2/3}}\left[-b^{2/3}\ln(b - x^3) - a\ln\frac{b^{1/3} - x}{\sqrt{b^{2/3} + b^{1/3}x + x^2}}\right.$$

$$\left. + \sqrt{3}\, a \tan^{-1}\frac{\sqrt{3}\, x}{2b^{1/3} + x}\right]_{1-\lambda}^{1} \qquad 2.6.2$$

To maximize U_l^2, the value of F must be as large as possible, which means the integration of f over λ, to which F is proportional, should extend over as large a range as possible. In terms of relation 2.6.2 this means that $\lambda_{\infty-}$ should be unity and thus the lower limit of the

bracket in relation 2.6.2 should be zero. Pointed cones are thus indicated as having the highest limiting velocities. As $a \to 0$, the limiting velocity indicated by relation 2.6.2 approaches the value which, as will be shown below, corresponds to a cylinder. At the other extreme of $a \to \infty$, corresponding to a blunt cone of zero altitude, the limiting velocity approaches the form

$$U_l^2 = 4g\left(\frac{\Delta W}{\eta}\right)\frac{1}{b^{2/3}}\left[\sqrt{3}\tan^{-1}\frac{\sqrt{3}}{1+2b^{1/3}} - \ln\frac{b^{1/3}-1}{\sqrt{b^{2/3}+b^{1/3}+1}}\right] \qquad 2.6.3$$

This result must be given a cautious physical interpretation. On the present model there is no loss of material from the flanks and so the drag of the flanks is, in a sense, free. The relation 2.6.3, corresponding to the limiting shallow cone, puts the highest possible drag in the place where it costs nothing. This consideration also applies, in a weaker form, to the earlier result which indicated the pointed cone as yielding the highest limiting velocity. Only for flank slopes shallow enough that the flank heat input is truly small compared to the face input can the present model be considered valid. The infinitely shallow cone obviously does not meet this requirement. A quantitative estimate of the flank input is given in the appendix.

For the second integral with $\rho = 0$ at $\lambda = \lambda_{\infty}$ we find

$$\rho = \int_{\lambda}^{\lambda_{\infty}} \frac{d\lambda}{F(\lambda)} \qquad 2.6.4$$

A case of particular interest is that of a cylindrical body as a limiting form of the blunt cone. For cylinders, the parameter L goes infinite. Redefining λ as l/l_0 and l_0 as L(λ_{∞} is thus always unity) one finds

$$\left.\begin{aligned} C_D A &= \frac{\pi}{2} D^2 \\ V &= \frac{\pi}{4} D^2 L \lambda \\ f(\lambda) &= \frac{g h_s'}{wL}\left(\lambda + \frac{\mu}{1-\mu}\right)^{-1} \end{aligned}\right\} \qquad 2.6.5$$

The function F is

$$F(\lambda) = \frac{2gh_s'}{wL} \ln\left(1 + \frac{1-\mu}{\mu} \cdot \lambda\right) \qquad 2.6.6$$

and the limiting velocity is given by

$$U_l^2 = 4g \cdot \frac{\Delta W}{\eta} \ln\left(\frac{1}{\mu}\right) \qquad 2.6.7$$

Since $C_D A$ has large values at every value of the weight, the cylinder yields high limiting velocities. The absence of D/L (now the diameter-length ratio) indicates no preferred proportions. Thus wafers and rods have the same limiting velocities.

The case of the homogeneous shrinking sphere was treated in reference 8. If this spherical configuration is formally converted to a space probe by addition of a point mass at the center, the function f is

$$f(\lambda) = \frac{3gh_s'}{8wR} \cdot \frac{\lambda^2}{\lambda^3 + \frac{\mu}{1-\mu}} \qquad 2.6.8$$

where $\lambda = \frac{r}{R}$ and $R = r_{\infty-}$. An integration yields

$$F(\lambda) = \frac{gh_s'}{4wR} \ln\left(\frac{1-\mu}{\mu} \cdot \lambda^3 + 1\right) \qquad 2.6.9$$

and for the limiting velocity

$$U_l^2 = 2g\left(\frac{\Delta W}{\eta}\right)\ln\left(\frac{1}{\mu}\right) \qquad 2.6.10$$

The limiting velocity for the modified Hansen's solution is thus $\sqrt{2}^{-1}$ or 0.707 times the limiting velocity for the flat-faced cylinders. Again, as in the case of the cones and cylinders, there is no size dependency.

CHAPTER III

DISCUSSION OF ANALYTICAL RESULTS

3.1 Meteor-Like Bodies

The case of meteor-like bodies appears in the present analysis as the limiting case of vanishing payloads, $\mu \to 0$. In this limit, for all three kinds of bodies considered (the blunted cones, the cylinders, and Hansen's sphere) the limiting velocity becomes infinite. Even when the experimental heat input function corresponding to $r = 2$, $s = 14$ is allowed unrestricted action it can be shown that the limiting velocity becomes infinite as $\mu \to 0$. To obtain finite values of limiting velocity at $\mu = 0$, one must use a value of $\lambda_{\infty+} > 0$ as the defining value.

3.2 Energy Ratios

A convenient way of considering the heat inputs for atmospheric entry is in terms of the initial kinetic energy of the body. For entries at limiting velocity the heat capacity of the body, $H_{\infty-}$, divided by the initial kinetic energy of the body, $T_{\infty-}$, at limiting velocity indicates the fraction of the initial kinetic energy of the body, returned to the body as heat under the most extreme conditions of survival. In the case of the flat-faced cylinders which yielded high values of limiting velocity for the class of probes considered in the present analysis, the ratio is found to be

$$\frac{H_{\infty-}}{T_{\infty-}} = \frac{1}{2}(1 - \mu)\frac{\eta}{\ln\left(\frac{1}{\mu}\right)} \qquad 3.2.1$$

Again, there is singular behavior for the case $\mu \to 0$ corresponding to meteor-like bodies. The ratio $\frac{H_{\infty-}}{T_{\infty-}}$ can be made arbitrarily small for small enough values of μ. The singular behavior of limiting velocity as the payload vanishes emphasizes the distinction between the cases of meteor and probe entry.

3.3 Effects of Shape and Size

According to the analysis there is no effect of size on limiting velocity, at least for the limiting form of the heat function. The only effect of increasing size is a lower altitude for the high mass-loss region. On a limiting trajectory all the volume must be consumed, on the present model, and if more volume is provided a longer path is required for complete consumption when the initial velocity is the same in every case. The diameter-length ratio of the cylinder does not affect the limiting velocity. The cylinder is not the only shape with the same high limiting velocity. For example, a flat-faced pointed cone, traveling base foremost has the same limiting velocity as does the cylinder. The key requirement is a high value of the integral

$$\int_0^{\lambda_{\infty-}} \frac{d\lambda}{\delta}$$

or in other words, a high value of the mean reciprocal ballistic parameter with respect to the changing size of the vehicle. This may be more clearly seen perhaps, if the ratio of equation 1.1.6 to equation 2.3.11 is taken yielding

$$\frac{-\frac{dU}{d\omega}}{-\frac{d\lambda}{d\omega}} = \frac{\frac{gh_s'}{2\delta}\rho U}{\frac{h_s'}{w}\frac{\eta}{\Delta W}\frac{}{2L}\rho U^2} \qquad 3.2.2$$

or

$$d(U^2) = 2g \frac{\Delta W}{\eta} \frac{wL}{\delta} d\lambda \propto \frac{d\lambda}{\delta} \qquad 3.2.3$$

which shows the advantage of small δ expressed in a differential form.

CHAPTER IV

NUMERICAL RESULTS

4.1 Limiting Velocities

For the cones and cylinders the value $D/L = 0.3$ has been adopted in the calculations. In the case of the cone this value yields a sufficiently slender shape that the convection to the flanks is small (see appendix). The value $h_s' = 25{,}200$ feet has been used throughout. This value corresponds to vertical entry into the atmosphere. The formulas of the analysis indicate the scaling with h_s'. For example, the air loading, G, varies inversely with h_s'.

The limiting velocities indicated by the analysis for the limiting heat function are indicated in figure 3. Certain cases may be cited as examples. With a cylinder made of a material such as graphite ($\Delta W \approx 15{,}000$ Btu/lb), a payload fraction of $e^{-1} = 0.368$, and $\eta = 1/2$, the indicated limiting velocity is about 55,000 feet per second, which is about the launch speed for escape from the solar system. For the perhaps more reasonable η value of 1/4, the limiting value jumps to 78,000 feet per second, some 40 percent higher than launch speed for solar system escape, and well beyond the 50,000 to 60,000 feet per second range suggested in reference 2. The unbounded nature of limiting velocity with vanishing payload implies that there is, in principle, no limit to the payload size or entry speeds possible. The payload fraction need only be decreased to that corresponding to the desired entry velocity and a large enough probe constructed that the assumed fractional value is realized.

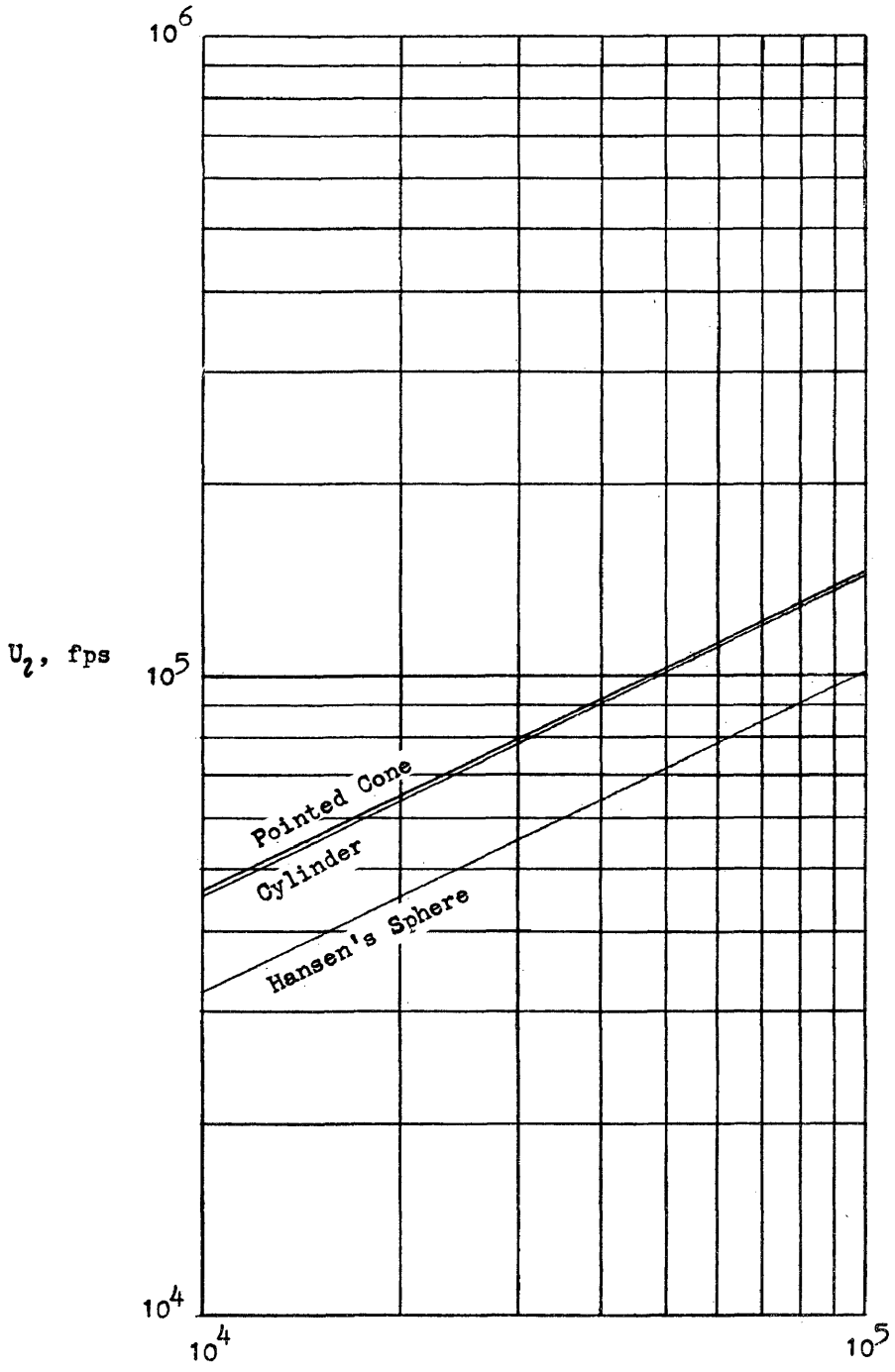

(a) $\mu = 1/8$.

Figure 3.- Limiting velocity for various probes.

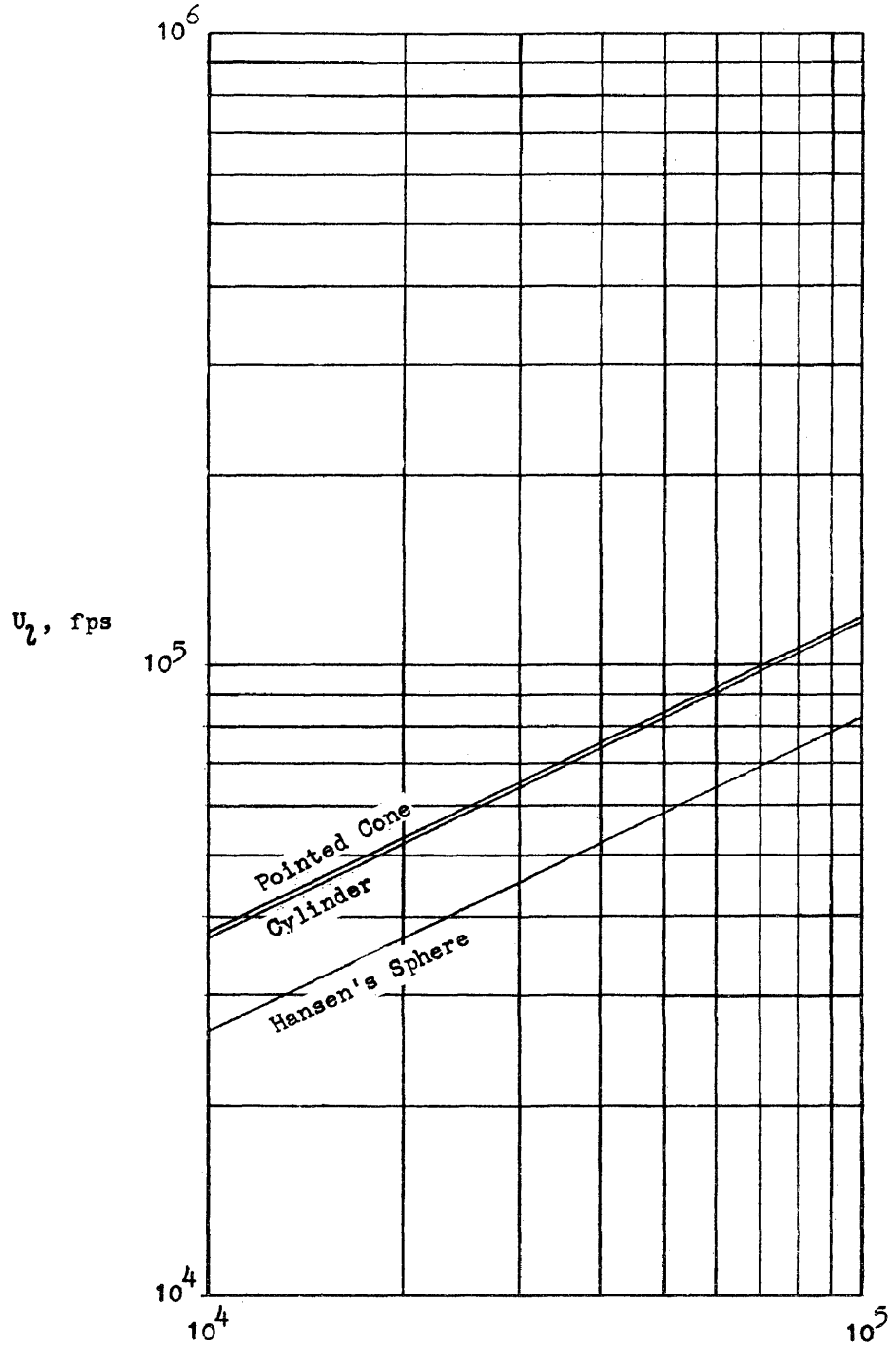

(b) $\mu = 1/4$.

Figure 3.- Continued.

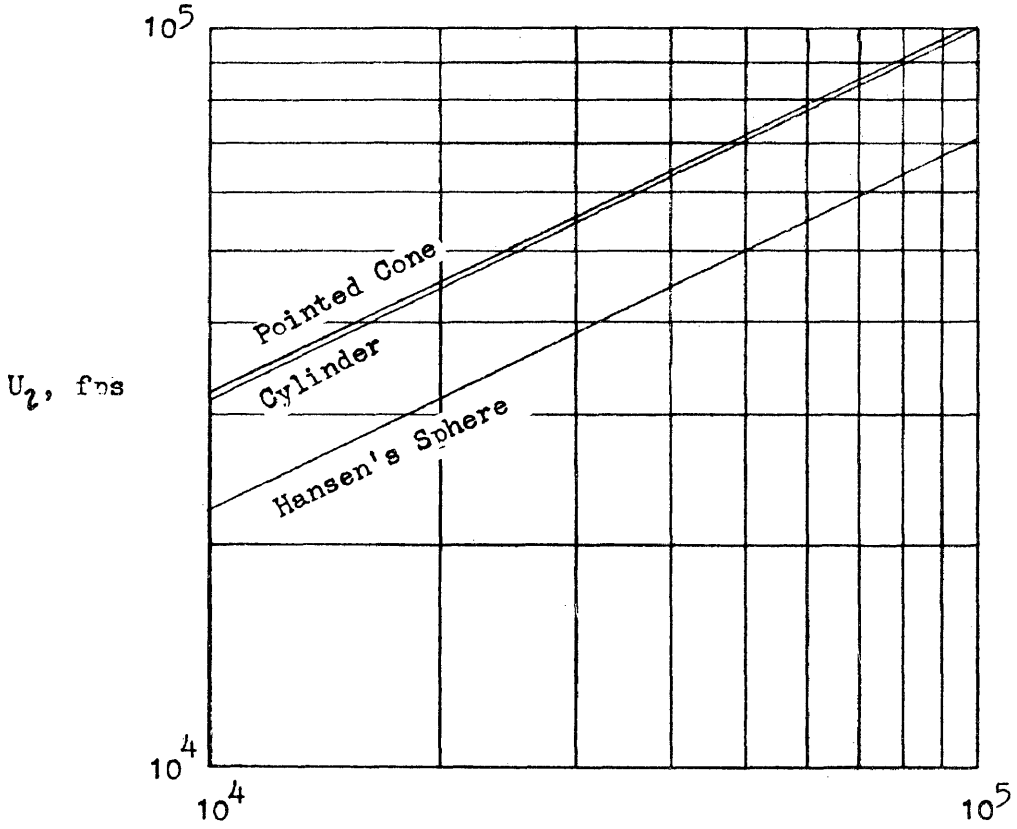

(c) $\mu = e^{-1}$.

Figure 3.- Continued.

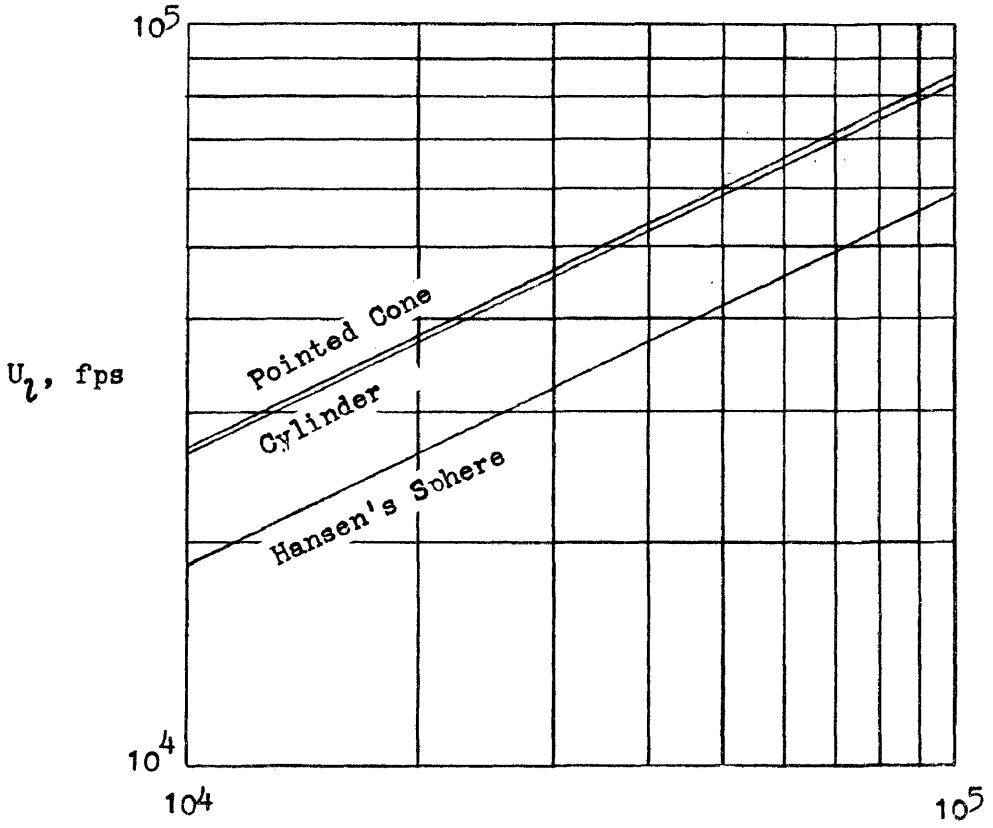

(d) $\mu = 1/2$.

Figure 3.- Concluded.

Aside from the fact that there are practical limits on the size of probe which may be launched, there is, more fundamentally, the limited thickness of the earth's atmosphere to be considered.

4.2 Limiting Sizes

With increasing probe size the position of the high mass-loss region moves to lower altitudes. It should be recalled, however, that the air loads or limiting velocity do not change with size. A convenient reference point near the end of the high mass-loss region is the peak G point. For some size of probe the peak G point will occur at sea-level density ($\omega = -6.03$ in English units). For sizes larger than that which puts the peak G point at sea-level survival is clearly impossible. In figure 4 the size limitation imposed by the finite depth of the atmosphere is indicated in terms of the location of the peak G point as a function of size and payload fraction with $w = 140$ psf. For weight densities other than 140 psf, figure 4 applies if the actual value of L is multiplied by $w/140$. The characteristic length used for Hansen's sphere is the diameter, 2R. It should be noted that, if one dismisses the case of the shrinking sphere as a probe model, there is a definite bound on the size of probe that can make a limiting entry for $\mu < 1/2$. This limit is in the neighborhood of $L = 10$ feet, which for a material such as graphite ($w \approx 140$ psf), indicates a probe weight of about 10^4 pounds for a cylinder 10 feet long and 3 feet in diameter. Increasing the diameter does not affect the position of the high mass-loss region or the limiting velocity. Increasing the effective heat capacity, $\Delta W/\eta$, does not affect the limiting size either, but does, as shown in figure 3, raise the limiting velocity.

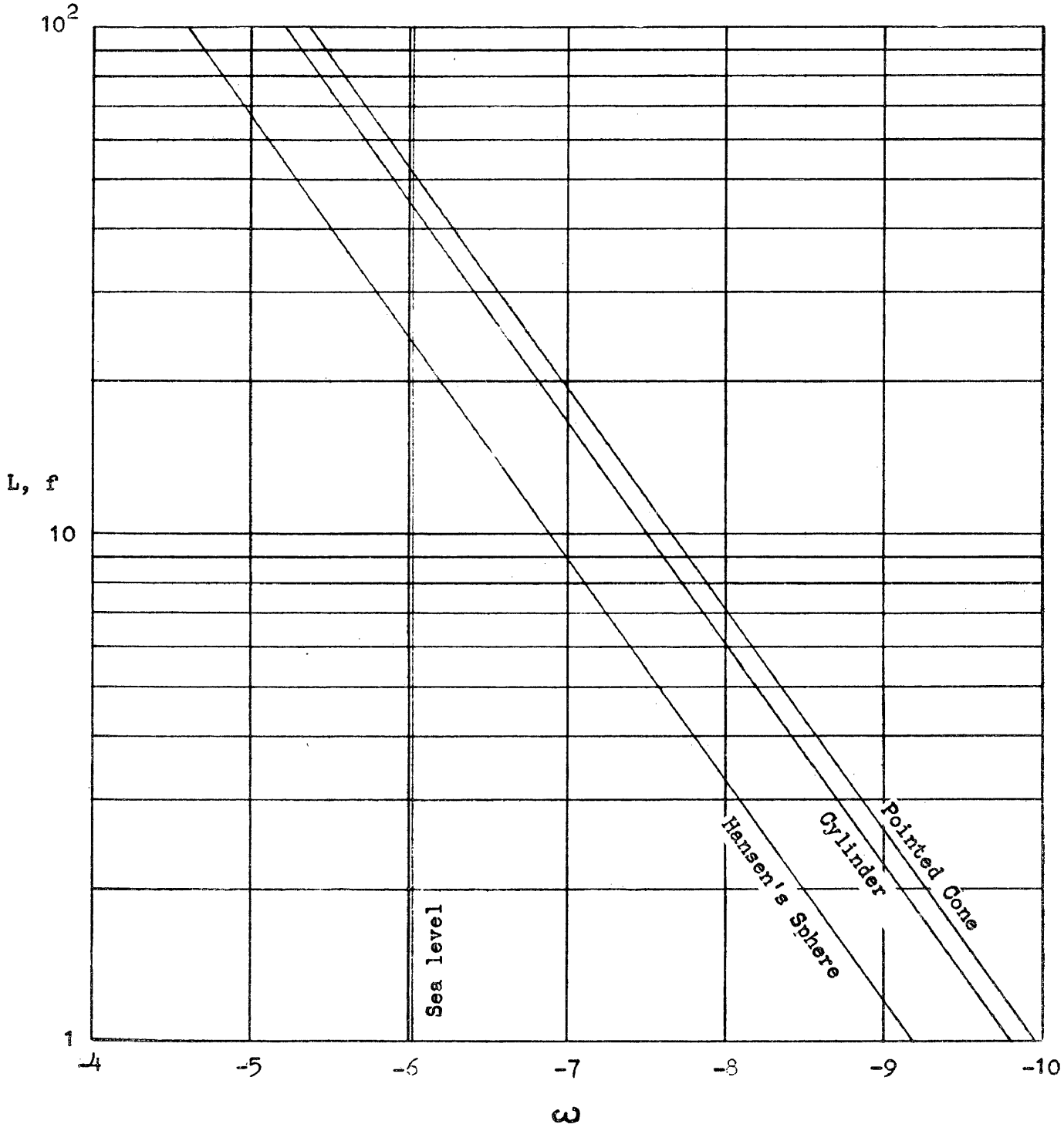

(a) $\mu = 1/8$.

Figure 4.- Location of peak G point for various probes.

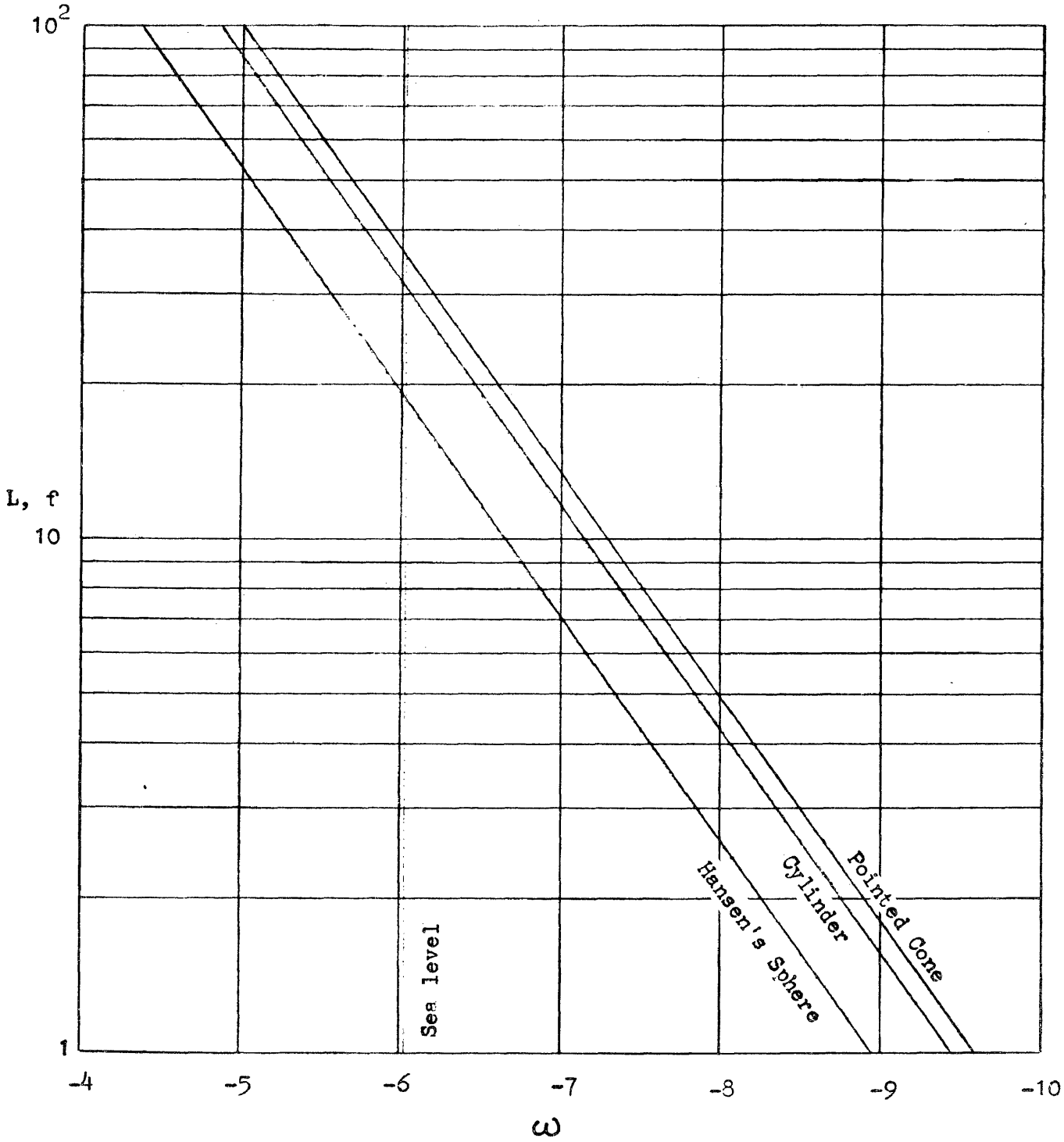

(b) $\mu = 1/4$.

Figure 4.- Continued.

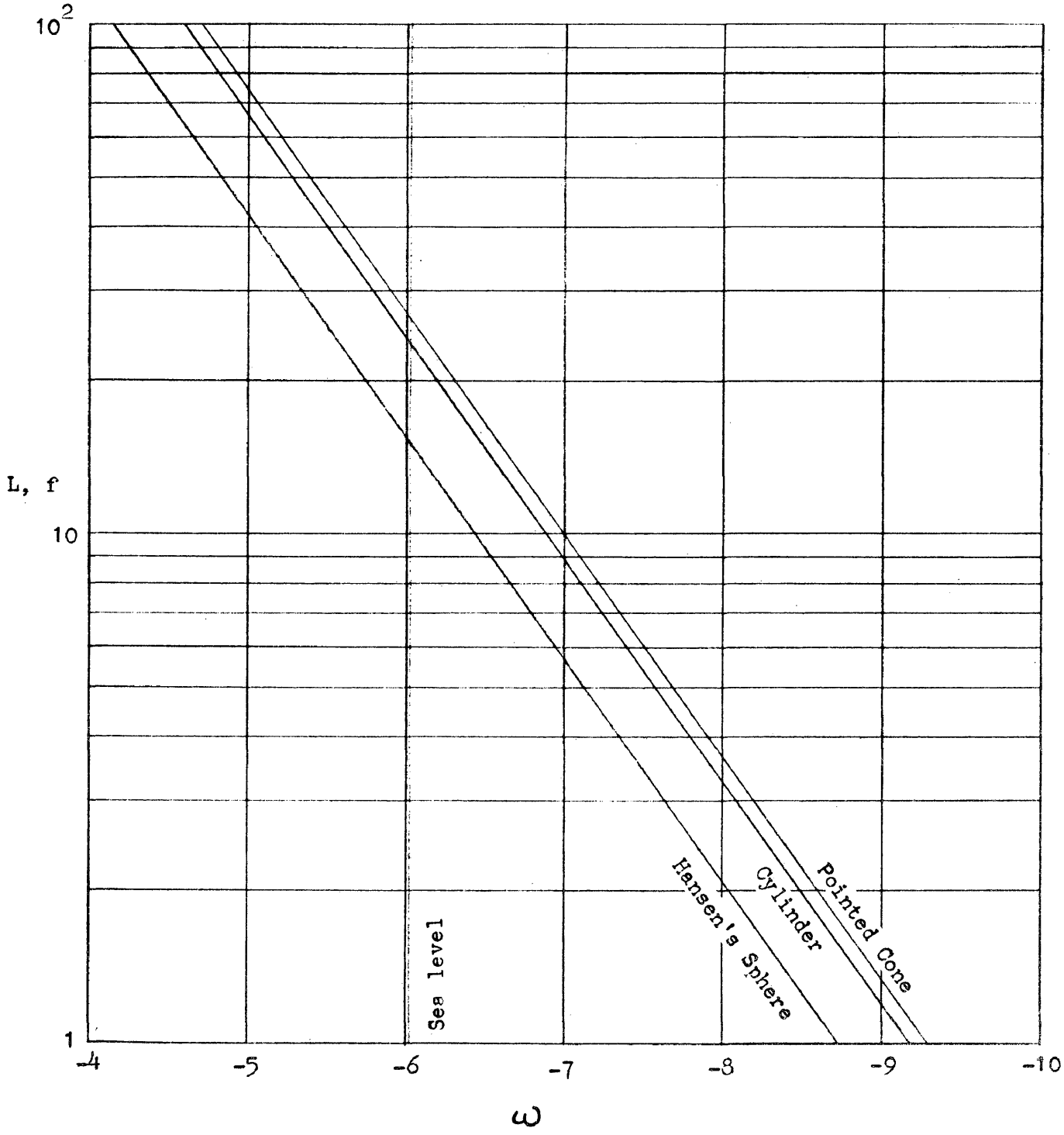

(c) $\mu = e^{-1}$

Figure 4.- Continued.

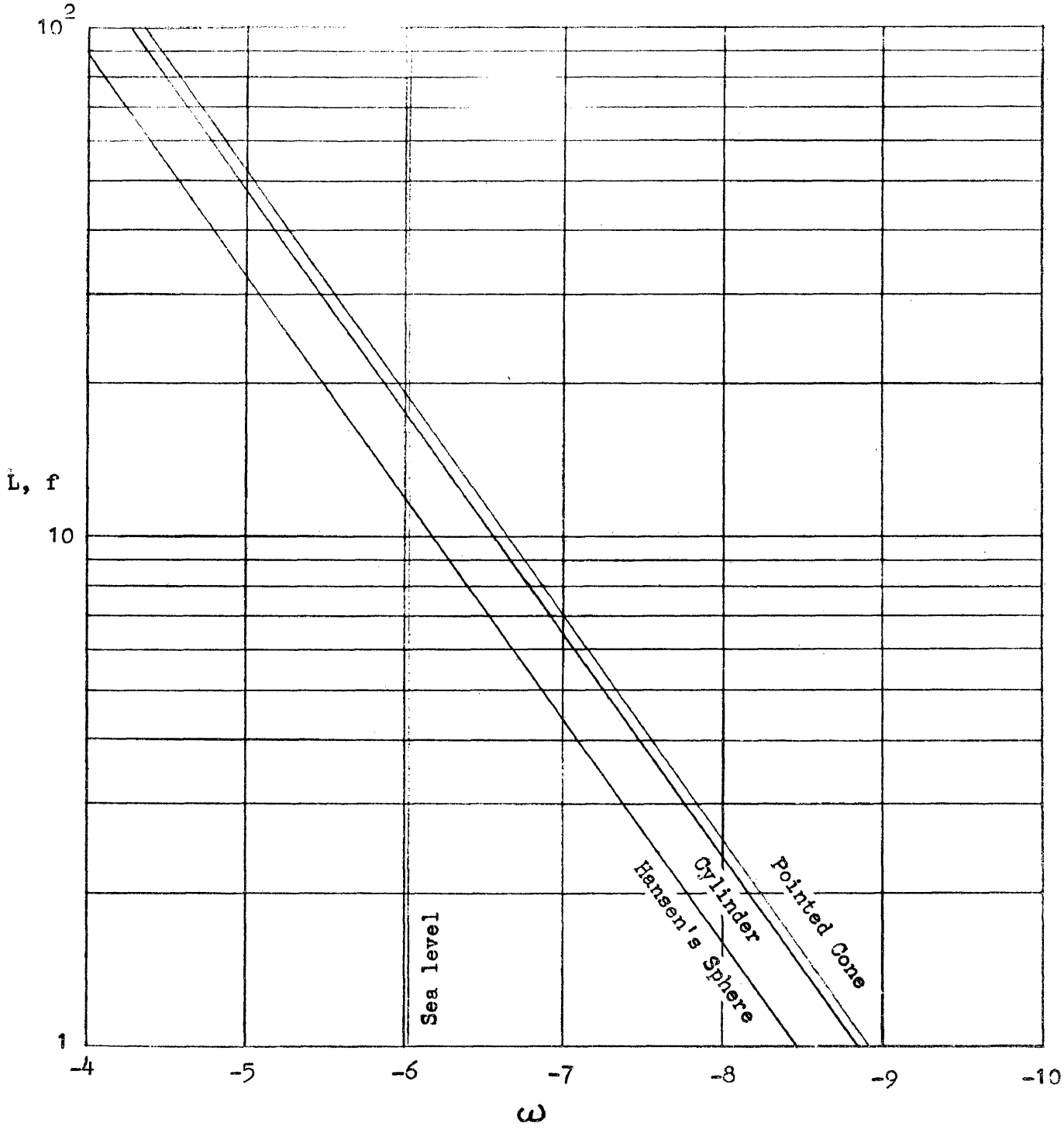

(d) $\mu = 1/2$.

Figure 4.- Concluded.

4.3 Peak G Values

The values of peak G are indicated in figure 5 for a range of values of $\Delta W/\eta$, the effective heat capacity. The peak G value (and all other G values) are proportional to the quantity $\Delta W/\eta$. Limiting velocity is thus unbounded for unlimited increase in effective heat capacity as well as for vanishing μ. However, the position of the high mass-loss region does not shift with $\Delta W/\eta$, but rather with size, L, as already shown in figure 4. Although the pointed cone of $D/L = 0.3$ has only a slightly higher limiting velocity than does the cylinder it is subject to considerably higher loadings. These higher loadings are associated with the absence of high C_pA values until late in the trajectory for the case of the pointed cone.

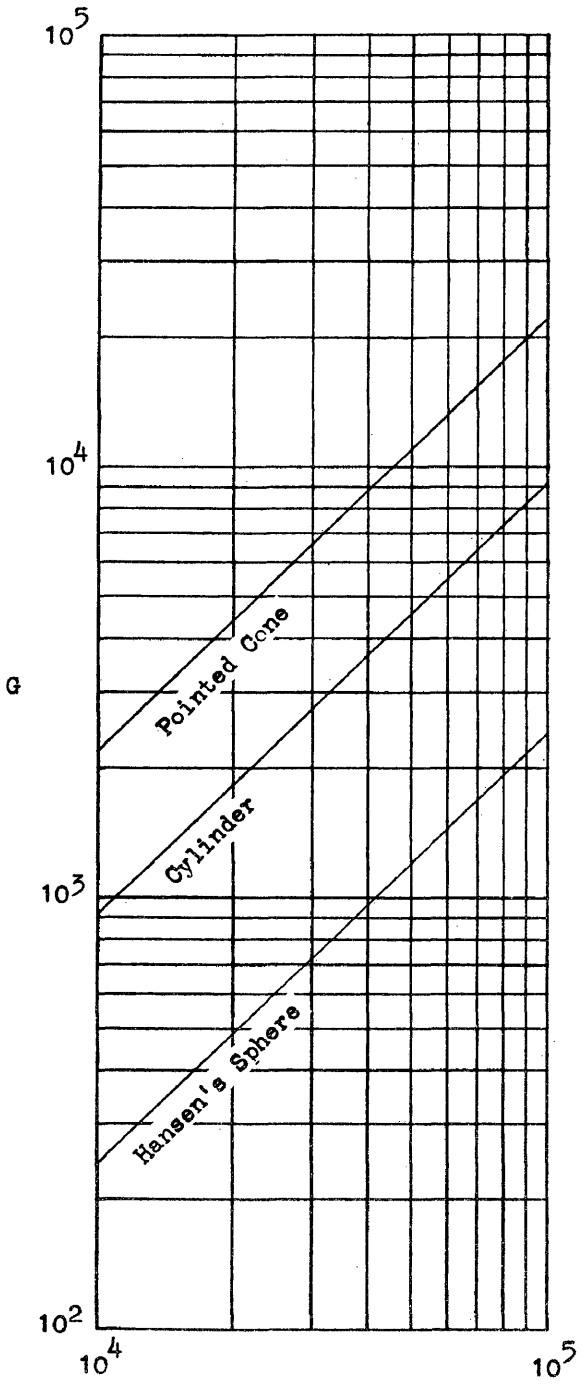

(a) $\mu = 1/8$.

Figure 5.- Value of peak G for various probes.

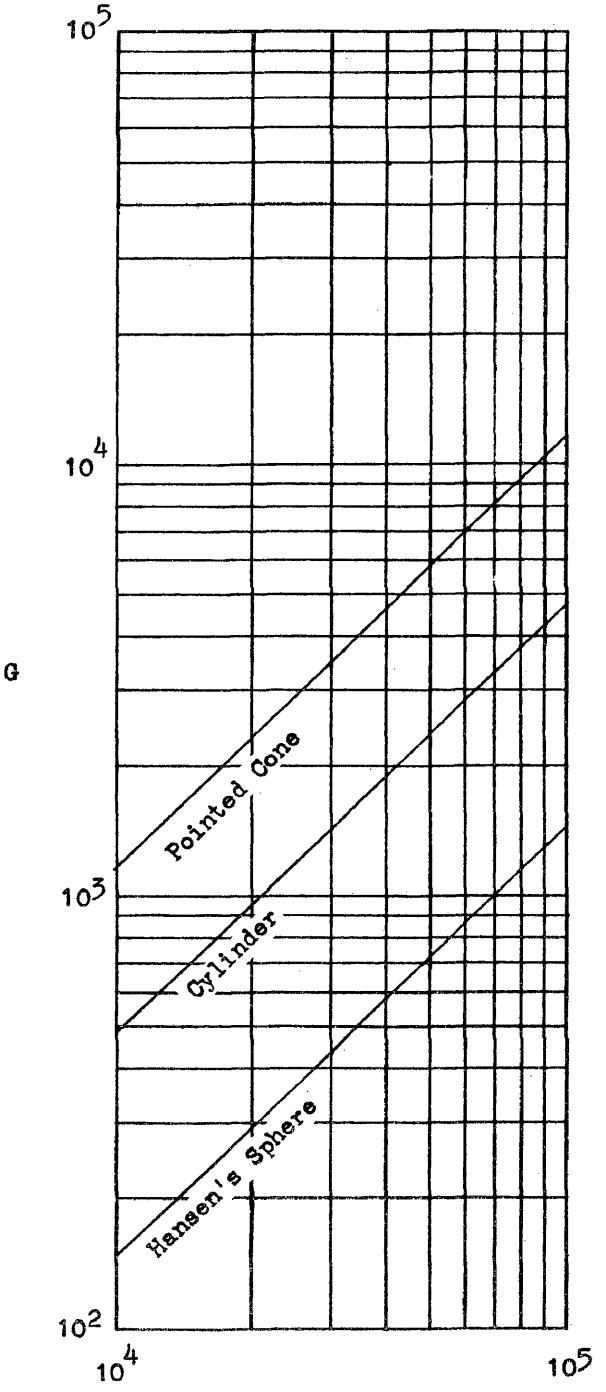

(b) $\mu = 1/4$.

Figure 5.- Continued.

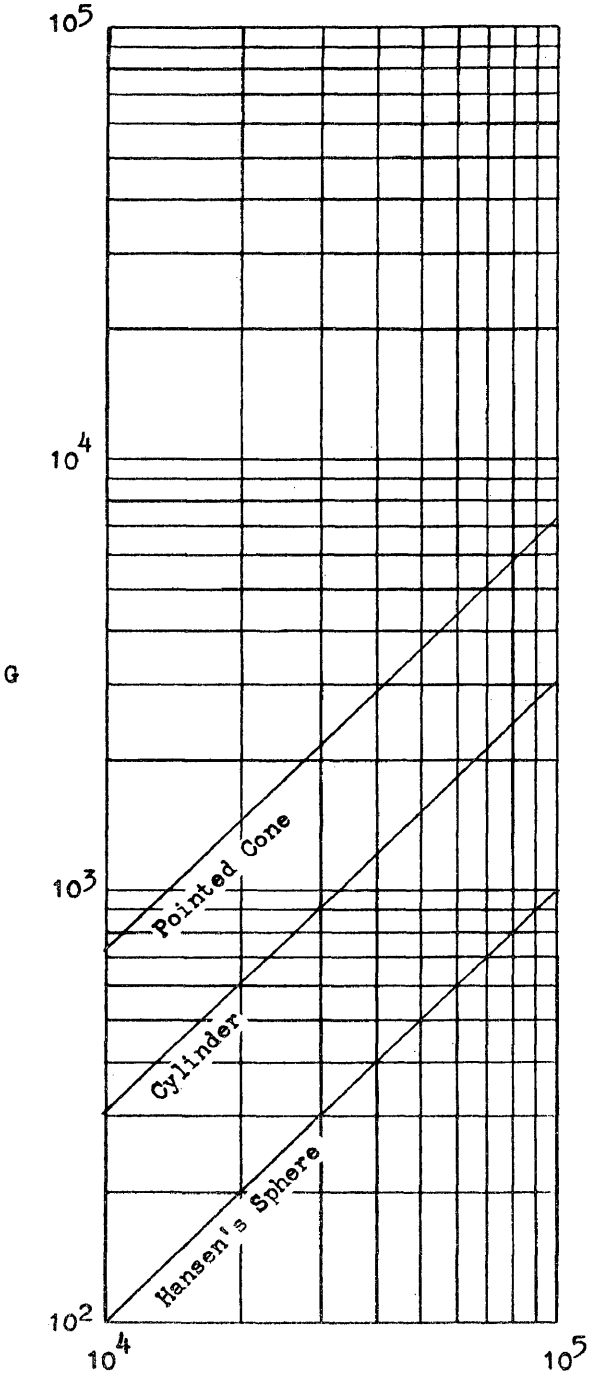

(c) $\mu = e^{-1}$.

Figure 5.- Continued.

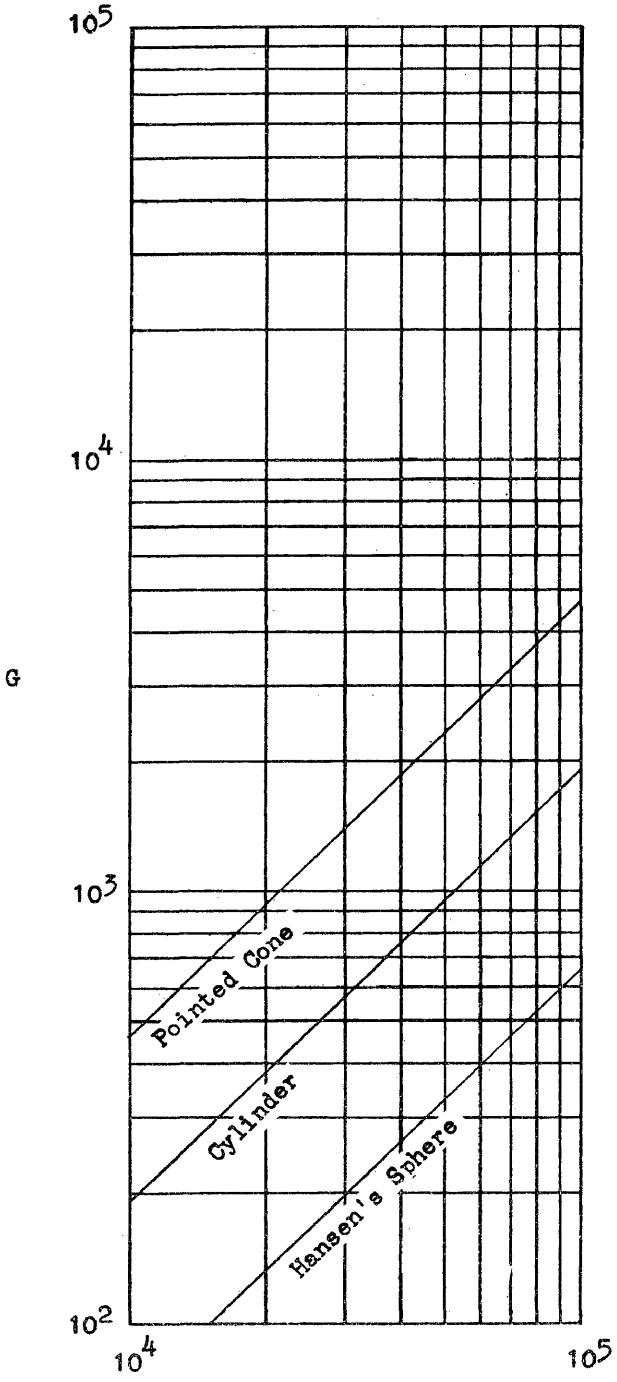

(d) $\mu = 1/2$.

Figure 5.- Concluded.

CHAPTER V

CONCLUDING REMARKS

The analysis has shown that, for a limiting heat input function and a simple probe model, there is no limit to the size of probe that may survive entry to the earth's atmosphere save that imposed by the finite depth of the atmosphere. In the absence of a payload there was found to be no limit to the possible entry speed. The zero-payload case corresponds to that of meteor entry. For finite payload fractions, entry speeds considerably in excess of the launch speed for solar system escape were found to be possible.

The form of probe for highest entry speed was expected to be slender. This expectation was borne out when the analysis indicated slender pointed cones as having the highest value of limiting speed for the class of probes considered. However, the entry speed for cylinders was nearly as high, and was independent of the cylinder proportions, so that wafers and rods have the same values. The indicated slight advantage of the slender cone was thought to come, in part at least, from the form of the analytical model and not from any real physical advantage. In sum, for the extreme case of high mass-loss entries there is, on the present analysis, no clear indication of desirable proportions. The fact that high entry speeds were found for the cylindrical probes suggests that the blunt body indicated for low mass-loss entries in which convective heat

transfer is dominant may again be suitable in the extreme case of high mass-loss entries in which radiative heat transfer is dominant.

INDEX OF SYMBOLS

Symbols	Definition	Paragraph
ρ	mass density of air	1.1
h	altitude	
h_s	scale height	
h'_s	generalized scale height	
γ	flight-path angle	
t	time	
U	air velocity	
g	acceleration of gravity	
m	mass of probe	
δ	ballistic parameter	
C_D	drag coefficient	
A	reference area	
λ	nondimensional size (fig. 2)	
$f(\lambda)$	ballistic function	
r,s	exponents in heating rate function	1.2
$g(\lambda)$	heating function	
p	slope, $\frac{d\lambda}{d\rho}$	1.3
π	slope, $\frac{d\lambda}{d\omega}$	
ω	natural logarithm of ρ	
ω'	ω value for translated integral curve	
σ	amount of translation of integral curve	

Symbols	Definition	Paragraph
z	parameter to which $f(\lambda)$ is proportional	1.3
z'	transformed value of z	
sub $\infty+$	$\omega = \infty$	
sub $\infty-$	$\omega = -\infty$	
$\dot{Q}$	heat input per unit frontal area	1.4
η	fraction of kinetic energy flux converted to heat	
x	characteristic length	
q	heat input per unit surface area	
sub s	stagnation point	
sub c	convective	
sub r	radiative	
D/2L	tangent of cone half angle (fig. 2)	2.2
V	volume of probe	
m_f	point payload mass	
w	weight density of probe volume	
L	length of cone (fig. 2)	
μ	payload fraction	
super .	derivative with time	2.3
ΔW	heat of sublimation	
S	surface area	
$\tilde{q}/q_s$	ratio of mean to stagnation point heating rates	
α, β	constants in heating rate functions	
K	parameter product for experimental heating function	
K'	parameter product for limiting heating function	
$F(\lambda)$	first integral of f	2.4

Symbols	Definition	Paragraph
U_l	limiting velocity	2.4
G	deceleration in units of g	2.5
r	radius of sphere	2.6
R	radius of sphere at $\omega = -\infty$	
H	heat capacity of probe	3.2
T	kinetic energy of probe	

APPENDIX

PROPERTIES OF TRAJECTORIES CORRESPONDING TO $g(\lambda) = K(1 - \lambda)$

As mentioned earlier, the experimental variation of radiative heating obtained from reference 4 which indicates $r = 2$, $s = 14$, leads to excessive values of radiation heating at the densities and speeds of high mass-loss entries. However, the analysis holds for other values of r and s as long as the stagnation point heating rate is proportional to the size of the face. The trajectory properties corresponding to $g(\lambda) = K(1 - \lambda)$ thus may have some future interest. Under a σ-z shift the following functional relations are found:

$$\left(\frac{w}{h_s'}\right)^{r-1} \cdot \left(\frac{L}{g}\right)^{r} \cdot U^{s-1} = \text{constant}$$

$$G \cdot (L)^{\frac{2r}{s-1}} \cdot (w)^{\frac{2(r-1)}{s-1}} \cdot (g)^{1 - \frac{2r}{s-1}} \cdot (h_s')^{1 - \frac{2(r-1)}{s-1}} = \text{constant} \qquad \text{(A-2)}$$

so that, specifically

$$\frac{\partial \log U}{\partial \log L} = - \frac{r}{s - 1} \qquad \text{(A-3)}$$

$$\frac{\partial \log G}{\partial \log L} = - \frac{2r}{s - 1} \qquad \text{(A-4)}$$

For limiting velocities there is thus a size effect favoring smaller sizes, which might be expected, since the heating per unit area is proportional to size, on the assumed heat input function.

In the case of the limiting heat function for which $g(\lambda) = K'$ the heating per unit area is independent of size and there is no size effect on limiting velocity. The position of the high mass-loss region moves independently of the heat function according to the condition

$$\rho \cdot \frac{gh_s'}{wL} = \text{constant} \tag{A-5}$$

or

$$\frac{\partial x_0}{\partial \ln \frac{wL}{gh_s'}} = 1 \tag{A-6}$$

The effect of an increase in size is to put the high mass-loss region at lower altitudes. Since the effects of changes in w, g, h_s' are equivalent to size changes according to equation (A-6), the term size change includes the effects of changes in w, g, h_s', the direction of the equivalent change being indicated by equation (A-6). In the direction of smaller sizes, the effect of convection will become relatively more important since the ratio of convective heating to radiative heating rates increases as $\sqrt{\rho}^{-1}$ on the limiting form of the heat function and at a higher rate on the experimental variation of reference 4. If the convective input to the face is regarded as a perturbation and evaluated at every point of a trajectory established under radiation dominance the limits of radiation dominance may be found. The convective heating rate to the face is

$$\dot{Q}_c = \frac{\pi}{4}\frac{D}{L}^{3/2}\left(\frac{\dot{q}}{q_s}\right)_c \alpha \rho^m U^n L^{3/2}(1-\lambda)^{3/2} \tag{A-7}$$

The integrated convective input to the face of the blunted cones is thus

$$Q_c = \frac{\pi}{4} h_s'\left(\frac{\dot{q}}{q_s}\right)_c \alpha \frac{D}{L}^{3/2} L^{3/2} \int_{-\infty}^{\infty} \rho^m U^{n-1} \cdot (1-\lambda)^{3/2} \cdot d\omega \tag{A-8}$$

The ratio of convective to radiative inputs for limiting trajectories is found as

$$\frac{Q_c}{Q_r} = 3\frac{h_s'}{w\,\Delta W}\left(\frac{\dot{q}}{q_s}\right)_c \alpha \sqrt{\frac{D}{L}}^{-1} L^{-3/2}\left\{1 - (1-\lambda_{\infty-})^3\right\}^{-1} \int_{-\infty}^{\infty} \rho^m U^{n-1}(1-\lambda)^{3/2} \cdot d\omega \tag{A-9}$$

When the ratio $\frac{Q_c}{Q_r}$ is evaluated for one limiting trajectory it can be scaled to all other values of L by applying the σ-z change which yields the following scaling laws:

$$\frac{\partial \log Q_r}{\partial \log L} = 3 \tag{A-10}$$

$$\frac{\partial \log Q_c}{\partial \log L} = \frac{3}{2} + m - \frac{(n-1)r}{s-1} \tag{A-11}$$

$$\frac{\partial \log \frac{Q_c}{Q_r}}{\partial \log L} = -\frac{3}{2} + m - \frac{(n-1)r}{s-1} \tag{A-12}$$

Using equation (A-12) and the value of $\frac{Q_c}{Q_r}$ for a single trajectory one may extrapolate to find the L at which $Q_c \sim Q_r$. The ratio $\frac{Q_c}{Q_r}$ is

$$\frac{Q_c}{Q_r} = \frac{h_s'}{w\,\Delta W} \cdot \left(\frac{\bar{q}}{q_s}\right)_c \alpha \sqrt{\frac{D}{L}}^{-1} L^{-3/2} \int_{-\infty}^{\infty} \rho^m U^{n-1} d\omega \qquad \text{(A-13)}$$

with the corresponding scaling laws

$$\frac{\partial \log Q_r}{\partial \log L} = 3 \qquad \text{(A-14)}$$

$$\frac{\partial \log Q_c}{\partial \log L} = \frac{3}{2} + m \qquad \text{(A-15)}$$

$$\frac{\partial \log \frac{Q_c}{Q_r}}{\partial \log L} = -\frac{3}{2} + m \qquad \text{(A-16)}$$

For the cylindrical shapes on the heating function $g(\lambda) = K(1 - \lambda)$ there is an indicated choice of proportions which does not appear on the limiting function $g(\lambda) = K'$. If one considers a given amount of heat protection material, a volume constraint of the form

$$D^2 L = \text{constant} \qquad \text{(A-17)}$$

is implied. Regarding L as variable at constant volume, one finds on a σ-z change

$$L^{r - \frac{3}{2} U_l^{s-1}} = \text{constant} \qquad \text{(A-18)}$$

so that for $r > \frac{3}{2}$, $U_1 \to \infty$ for $L \to 0$ and the cylinder becomes an infinitely thin wafer of infinite diameter. For $r < \frac{3}{2}$, $U_1 \to \infty$ for $L \to \infty$ and the cylinder becomes an infinitely long needle of zero diameter. The high mass-loss regions for the two cases are at $\omega = -\infty$ for the wafer, and at $\omega = +\infty$ for the rod. On the limiting function $g(\lambda) = K'$, the limiting velocity was shown to be independent of the proportions.

On a limiting trajectory for the blunted cone at $L = 8$ with $\lambda_{\infty-} = 0.70$ the ratio $\frac{Q_c}{Q_r}$ is found to be 3.10^{-3}. After extrapolation to unit ratio by means of equation (A-12) the corresponding length is 3.10^{-2}. This length is small enough to be out of the range of conceivable probe sizes.

The relative size of the heat inputs to the face and to the flanks of the blunt cones can be roughly estimated. If, in the case of convection, the flank input is considered to be the same as that to a swept cylinder of variable radius and the loss of material on the flanks is neglected it turns out that

$$\frac{(Q_c)_{flanks}}{(Q_c)_{face}} < 1.6 \qquad \text{(A-19)}$$

so that the flank input is greater than, but comparable to, the face input. The regime of radiation dominance on the face thus implies dominance on the vehicle. If the radiative input to the flanks is put on the same basis as that to the face, in the case of the limiting heat input function, one finds, after integration, that

$$\frac{(Q_r)_{flanks}}{(Q_r)_{face}} < \frac{1}{2}\left(\frac{D}{L}\right)^2 \qquad \text{(A-20)}$$

where the energy input to the flanks is based on the component of the free-stream velocity normal to the flanks. For $\frac{D}{L} < 0.3$ the flank input is less than 5 percent of the radiative face input according to relation (A-20).

REFERENCES

1. Opik, Ernst J.: Physics of Meteor Flight in the Atmosphere. Interscience Publishers, 1958.

2. Riddell, Frederick R., Winkler, Howard B.: From ICBM Reentry to Meteorite Entry. Publication 61-113-1807, American Rocket Society. (National IAS-ARS Joint Meeting, June 13-16, 1961.)

3. Minzner, R. A., Champion, K. S. W., and Pond, H. L.: The ARDC Model Atmosphere, 1959. Air Force Surveys in Geophysics No. 115 (AFRC-TR-59-267) Air Force Cambridge Research Center, August 1959.

4. Lees, Lester: Laminar Heat Transfer Over Blunt-Nosed Bodies at Hypersonic Flight Speeds. Jet Propulsion, vol. 26, No. 4, April 1956, pp. 259-269.

5. Kivel, Bennett: Radiation From Hot Air and Stagnation Heating. AVCO Research Report 79, October 1959.

6. Thomas, P. D.: Air Emissivity and Shock-Layer Radiation. JAS Reader's Forum, April 1962.

7. Allen, H. Julian, and Eggers, A. J., Jr.: A Study of the Motion and Aerodynamic Heating of Ballistic Missiles Entering the Earth's Atmosphere at High Supersonic Speeds. NACA Report 1381, 1958.

8. Hansen, C. Frederick: The Erosion of Meteors and High-Speed Vehicles in the Upper Atmosphere. NACA TN 3962, March 1957.